Available online at www.sciencedirect.com
ScienceDirect
Polyhedron 26 (2007) 2165–2168
POLYHEDRON
www.elsevier.com/locate/poly

New Mn_3 structural motifs in manganese single-molecule magnetism from the use of 2-pyridyloximate ligands

Theocharis C. Stamatatos [a,b], Dolos Foguet-Albiol [b], Constantinos C. Stoumpos [a], Catherine P. Raptopoulou [c], Aris Terzis [c], Wolfgang Wernsdorfer [d], Spyros P. Perlepes [a,*], George Christou [b,*]

[a] *Department of Chemistry, University of Patras, GR 265 04 Patras, Greece*
[b] *Department of Chemistry, University of Florida, Gainesville, FL 32611-7200, USA*
[c] *Institute of Materials Science, NCSR "Demokritos", GR 153 10 Aghia Paraskevi Attikis, Greece*
[d] *Laboratoire Louis Néel-CNRS, 25 Avenue des Martyrs, 38042 Grenoble, Cedex 9, France*

Received 5 October 2006; accepted 13 October 2006
Available online 20 October 2006

Abstract

The use of 2-pyridyl oximes (L'H) in reactions with $[Mn_3^{III}O(O_2CR)_6(py)_3](ClO_4)$ has led to complexes $[Mn_3^{III}O(O_2CR)_3L'_3](ClO_4)$. Ferromagnetic exchange interactions between the three Mn^{III} ions in the complexes lead to spin ground states of $S = 6$. The complexes display the temperature- and scan rate-dependent hysteresis loops that are indicative of single-molecule magnetism behaviour.

Keywords: Ferromagnetic exchange; Manganese(III) carboxylate clusters; 2-Pyridyloximate ligands; Single-molecule magnets; Triangular oxide-centered complexes

The properties of conventional magnets are due to the collective behaviour of the unpaired electron spins of thousands or millions of individual metal ions in a particle or bulk material. Single-molecule magnets (SMMs) [1], on the other hand, are transition-metal, homo- or hetero-metallic clusters that individually exhibit the classical properties of a magnet below a critical temperature (the blocking temperature, currently ~4 K). Their properties arise from the combination of a large spin value (S) in the ground state and significant magnetoanisotropy of the easy-axis type (manifested as a negative zero-field splitting parameter, D). Due to their small size, SMMs have also been shown to exhibit interesting phenomena of the quantum world, such as quantum tunneling of magnetization [2] and quantum phase interference [3].

Compared to other 3d metal ions, manganese clusters are often characterized by large spin ground states; this characteristic, in combination with the Jahn–Teller distortion of high-spin Mn^{III} ions in near-octahedral stereochemistry (the source of the single-ion anisotropy) make manganese clusters ideal candidates for SMM behaviour. Thus, it is not surprising that the majority of SMMs are Mn(III) complexes of several nuclearities and various structural types, and often mixed valent, i.e. Mn(II/III) and Mn(III/IV) [1]. Despite this, there is a continuing need for Mn SMMs exhibiting new structural types to improve our understanding of this exciting phenomenon. Inspection of the literature reveals that there are no oxide-centered triangular Mn SMMs. Most of these triangular complexes have the general formula $[Mn_3O(O_2CR)_6L_3]^{0/+}$ (where L is a terminal ligand such as H_2O, MeCN, or pyridine) [4] and are often used as starting materials in SMM synthesis

* Corresponding authors. Tel.: +30 2610 997146; fax: +30 2610 997118 (S.P. Perlepes); tel.: +1 352 392 6737; fax: +1 352 392 8757 (G. Christou).
E-mail addresses: perlepes@patreas.upatras.gr (S.P. Perlepes), christou@chem.ufl.edu (G. Christou).

0277-5387/$ - see front matter
doi:10.1016/j.poly.2006.10.025

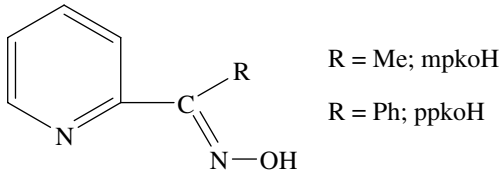

Fig. 1. The general formula of the 2-pyridyl oximes used in this work.

[1b]. The metal ions are antiferromagnetically coupled, and these complexes are not therefore SMMs. We are now pleased to report that the reactions of $[Mn_3^{III}O(O_2CR)_6(py)_3](ClO_4)$, where py is pyridine, with 2-pyridyl oximes (L′H) [5] give a family of oxide-centered triangular, ferromagnetically coupled $[Mn_3^{III}O(O_2CR)_3L'_3](ClO_4)$ complexes [6], which are the first triangular Mn SMMs. The ligands used are methyl 2-pyridyl ketone oxime (mpkoH) and phenyl 2-pyridyl ketone oxime (ppkoH); see Fig. 1.

Reactions of $[Mn_3O(O_2CMe)_6(py)_3](ClO_4)$ (**1**) with mpkoH, $[Mn_3O(O_2CEt)_6(py)_3](ClO_4)$ (**2**) with mpkoH, and $[Mn_3O(O_2CMe)_6(py)_3](ClO_4)$ (**1**) with ppkoH, in a 1:3 ratio in MeOH/MeCN gave dark brown solutions. These were evaporated to dryness under reduced pressure at room temperature, and the residues dissolved in CH_2Cl_2 and layered with *n*-hexane to slowly give dark brown crystals of $[Mn_3O(O_2CMe)_3(mpko)_3](ClO_4)\cdot 3CH_2Cl_2$ (**3**$\cdot 3CH_2Cl_2$), $[Mn_3O(O_2CEt)_3(mpko)_3](ClO_4)\cdot 1.2CH_2Cl_2\cdot 1.4H_2O$ (**4**$\cdot 1.2CH_2Cl_2\cdot 1.4H_2O$) and $[Mn_3O(O_2CMe)_3(ppko)_3](ClO_4)\cdot 2CH_2Cl_2$ (**5**$\cdot 2CH_2Cl_2$) in very good isolated yields (>70%). All three complexes gave very good analytical results.[1] The formation of the representative complex **4** can be summarized in the following balanced equation:

$$\underset{\mathbf{2}}{[Mn_3O(O_2CEt)_6(py)_3](ClO_4)} + 3mpkoH \xrightarrow{MeCN/MeOH/CH_2Cl_2} \underset{\mathbf{4}}{[Mn_3O(O_2CEt)_3(mpko)_3](ClO_4)} + 3EtCO_2H + 3py \quad (1)$$

The structure[2] of the cation of **3** (Fig. 2a) consists of an almost equilateral Mn_3^{III} triangle capped by the central oxide ion, O(61). Each edge of the triangle is bridged by a diatomic oximate group and an $\eta^1:\eta^1:\mu$-$MeCO_2^-$ group. The $mpko^-$ anions behave as $\eta^1{:}\eta^1{:}\eta^1{:}\mu$-ligands forming five-membered chelate rings. The oxide ion lies 0.295 Å above the plane defined by the three Mn^{III} ions. The coordination geometry of the metal ions is distorted octahedral. The O^{2-} character of O(61) and the Mn^{III} oxidation states were confirmed by charge considerations, bond lengths, bond valence sum (BVS) calculations [7] and the presence of Mn^{III} Jahn–Teller elongation axes [O(1)–Mn(1)–O(31), O(11)–Mn(2)–O(51), O(21)–Mn(3)–O(42)]. The trinuclear cations of complexes **4**$\cdot 1.2CH_2Cl_2\cdot 1.4H_2O$ (Fig. 2b) and **5**$\cdot 2CH_2Cl_2$ (Fig. S1) have very similar structures; their capping oxide ion lies 0.308 and 0.313 Å above the Mn_3^{III} plane, respectively.

Solid-state, direct current (DC) magnetic susceptibility (χ_M) data for dried **3**–**5** were collected in the temperature range 5.0–300 K in an applied field of 1 kG (0.1 T).[3] The $\chi_M T$ of **3** steadily increases from 13.01 $cm^3\,mol^{-1}\,K$ at 300 K to a maximum of 19.39 $cm^3\,mol^{-1}\,K$ at 30 K, before dropping to 17.41 $cm^3\,mol^{-1}\,K$ at 5.00 K (Fig. 3). This behaviour is indicative of ferromagnetic exchange between the metal centers resulting in an $S = 6$ ground state, with the low temperature decrease assigned to zero-field splitting, Zeeman effects and/or intermolecular antiferromagnetic interactions. The theoretical $\chi_M T$ (spin-only, $g = 2$) for $S = 6$ is 21 $cm^3\,mol^{-1}\,K$, close to the experimental value at 30.0 K. The data were fit to the theoretical expression for a Mn_3^{III} isosceles triangle [8]. The fit gave $J = +14.1\ cm^{-1}$, $J' = +3.8\ cm^{-1}$, $g = 1.91$, and 0.9% paramagnetic impurity term, assumed to be Mn^{II}. The corresponding fit values for **5** are $J = +31.1\ cm^{-1}$, $J' = +6.7\ cm^{-1}$, $g = 1.91$, and 1.5% paramagnetic impurity term.

In order to confirm the spin ground states of the complexes, magnetization data were collected in the ranges 1–70 kG and 1.8–10.0 K, and these are plotted as reduced magnetization ($M/N\mu_B$) versus H/T for **3** in Fig. 4. For a cluster entirely populating the ground state and experiencing no zero-field splitting, the isofield lines should superimpose and saturate at a $M/N\mu_B$ value equal to gS. The data were fit by matrix diagonalization to a model that assumes only the ground state is populated, includes axial zero-field splitting ($D\widehat{S}_z^2$) and the Zeeman interaction, and carries out a full powder average. The best fit (solid lines in Fig. 4) gave $S = 6$, $g = 1.92$ and $D = -0.34\ cm^{-1}$. The corresponding data for the other two complexes are $S = 6$, $g = 1.93$, $D = -0.34\ cm^{-1}$ for **4**, and $S = 6$, $g = 1.91$, $D = -0.36\ cm^{-1}$ for **5**.

The magnitude of S and sign of D suggested these complexes might be SMMs, and AC susceptibility studies were therefore carried out in the 1.8–10.0 K range in a 3.5 G field oscillating at frequencies up to 500 Hz. Frequency-dependent out-of-phase AC susceptibility signals were seen

[1] Elemental analyses: *Anal.* Calc. for $C_{27}H_{30}N_6O_{14}ClMn_3$ (**3**): C, 37.59; H, 3.50; N, 9.74. Found: C, 37.32; H, 3.49; N, 9.54%. *Anal.* Calc. for $C_{30}H_{38}N_6O_{15}ClMn_3$ (**4**$\cdot H_2O$): C, 39.04; H, 4.15; N, 9.11. Found: C, 39.24; H, 3.82; N, 9.07%. The dried complex **5**$\cdot 2CH_2Cl_2$ is hygroscopic and was analyzed as **5**$\cdot 3H_2O$. *Anal.* Calc. for $C_{42}H_{42}N_6O_{17}ClMn_3$ (**5**$\cdot 3H_2O$): C, 45.73; H, 3.84; N, 7.62. Found: C, 45.67; H, 3.26; N, 7.49%.

[2] Crystallographic data in brief: For complex **3**$\cdot 3CH_2Cl_2$: $C_{30}H_{36}N_6O_{14}Cl_7Mn_3$, 1117.64 g mol^{-1}, monoclinic, $P2_1/c$, $a = 12.986(5)$ Å, $b = 14.978(6)$ Å, $c = 23.150(10)$ Å, $\beta = 93.82(2)°$, $Z = 4$, $V = 4493(3)$ Å^3, $\rho_{calc} = 1.492$ g cm^{-3}, $T = 293(2)$ K, R_1 (on F) = 0.0696, wR_2 (on F^2) = 0.1936. For complex **4**$\cdot 1.2CH_2Cl_2\cdot 1.4H_2O$: $C_{31.2}H_{41.2}N_6O_{15.4}Cl_{3.4}Mn_3$, 1032.06 g mol^{-1}, monoclinic, $P2_1/c$, $a = 12.988(5)$ Å, $b = 15.111(6)$ Å, $c = 27.740(10)$ Å, $\beta = 94.82(1)°$, $Z = 4$, $V = 5425(4)$ Å^3, $\rho_{calc} = 1.264$ g cm^{-3}, $T = 293(2)$ K, R_1 (on F) = 0.0738, wR_2 (on F^2) = 0.2065. For complex **5**$\cdot 2CH_2Cl_2$: $C_{44}H_{40}N_6O_{14}Cl_5Mn_3$, 1218.92 g mol^{-1}, monoclinic, $P2_1/c$, $a = 13.566(2)$ Å, $b = 29.859(2)$ Å, $c = 26.085(3)$ Å, $\beta = 98.87(1)°$, $Z = 4$, $V = 10439.72(16)$ Å^3, $\rho_{calc} = 1.341$ g cm^{-3}, $T = 100(2)$ K.

[3] The magnetic behaviour of the three complexes is similar; detailed magnetic data are presented only for cluster **3**.

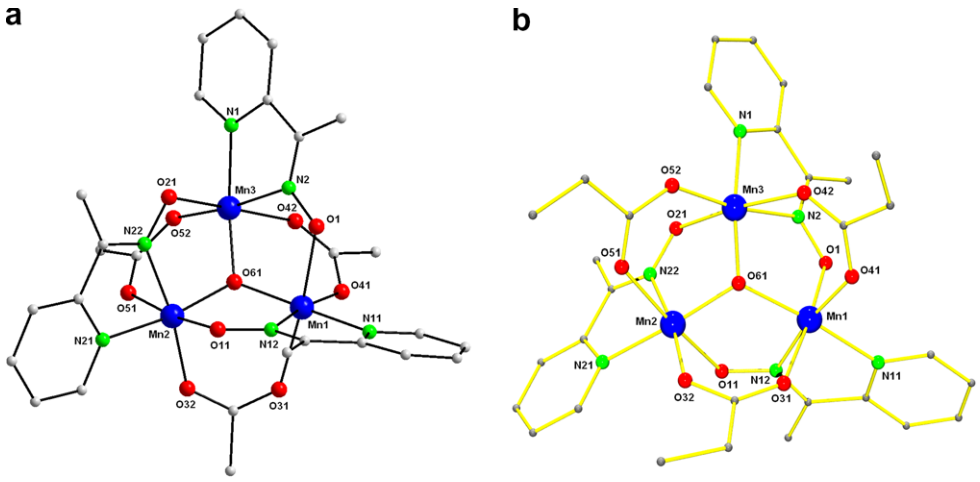

Fig. 2. Partially labeled plots of the trinuclear cations of (a) $\mathbf{3}\cdot 3CH_2Cl_2$ and (b) $\mathbf{4}\cdot 1.2CH_2Cl_2\cdot 1.4H_2O$.

for the three complexes below 3 K (but no peaks were observed) along with a concomitant decrease in the in-phase signal, indicative of SMM behaviour. The data for **4** are shown in Fig. 5.

In order to probe the possible SMM behaviour further, single-crystal hysteresis loop and relaxation measurements were performed for $\mathbf{3}\cdot 3CH_2Cl_2$ and $\mathbf{5}\cdot 2CH_2Cl_2$ using a micro-SQUID apparatus [9]. Fig. 6 presents typical magnetization (M) versus applied DC field measurements at 0.04 K for $\mathbf{3}\cdot 3CH_2Cl_2$. A hysteresis loop, the diagnostic property of a magnet, was observed below 1 K, whose coercivity increases with decreasing temperature and increasing field sweep rate, as expected for the superparamagnetic-like behaviour of an SMM. The loops show the step-like features indicative of quantum tunneling of magnetization (QTM) between M_s levels of the $S = 6$ ground state; the temperature-independent coercivity below 0.3 K indicates ground-state QTM. Magnetization decay versus time data and AC data to lower T were collected on

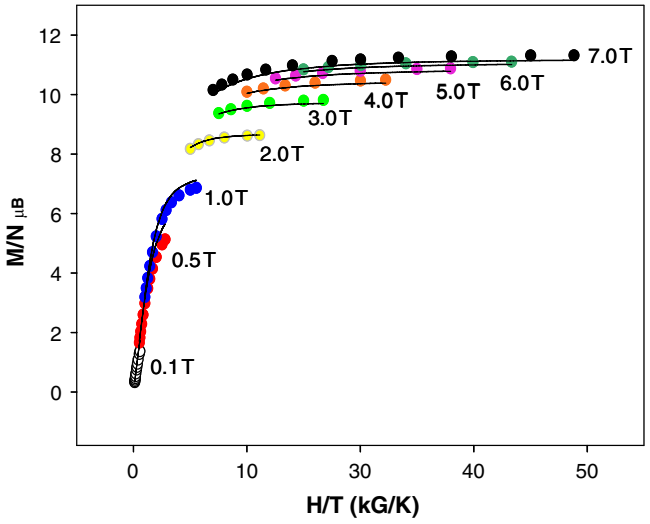

Fig. 4. Plot of the reduced magnetization, $M/N\mu_B$, vs. H/T for complex **3** at the indicated fields. The solid lines are the fit of the data; see the text for the fit parameters.

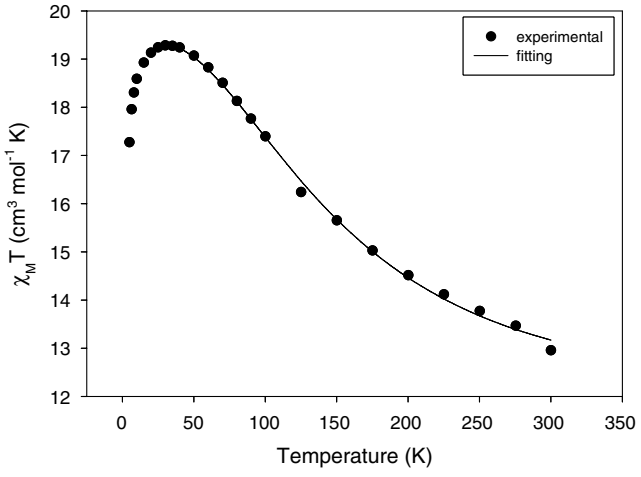

Fig. 3. $\chi_M T$ vs. T plot for complex **3** in the temperature range 5.0–300 K in a 1000 G (0.1 T) applied DC field; the solid line is the fit of the data (see the text for details).

$\mathbf{3}\cdot 3CH_2Cl_2$ and used to construct an Arrhenius plot (Fig. S2); fitting of the thermally activated region to the equation $\tau = \tau_0 \exp(U_{eff}/kT)$ gave $U_{eff} = 10.9$ K and $\tau_0 = 5.7\times 10^{-8}$ s, where U_{eff} is the effective magnetization relaxation barrier. Below 0.3 K, the relaxation is temperature-independent, consistent with relaxation by ground-state QTM. Slightly different SMM properties are observed for $\mathbf{5}\cdot 2CH_2Cl_2$ due to the presence of two crystallographically independent trinuclear cations in the crystal.[4]

An important question is the following: why are **3**–**5** ferromagnetically coupled and SMMs, whereas **1** and **2** (and many similar $[Mn_3O(O_2CR)_6L_3]^+$ complexes) are antiferromagnetically coupled and are not SMMs? A probable contributory factor is that **3**–**5** have their central oxide ligand ~0.3 Å above the Mn_3 plane due to the tridentate

[4] Details will be given in the full paper.

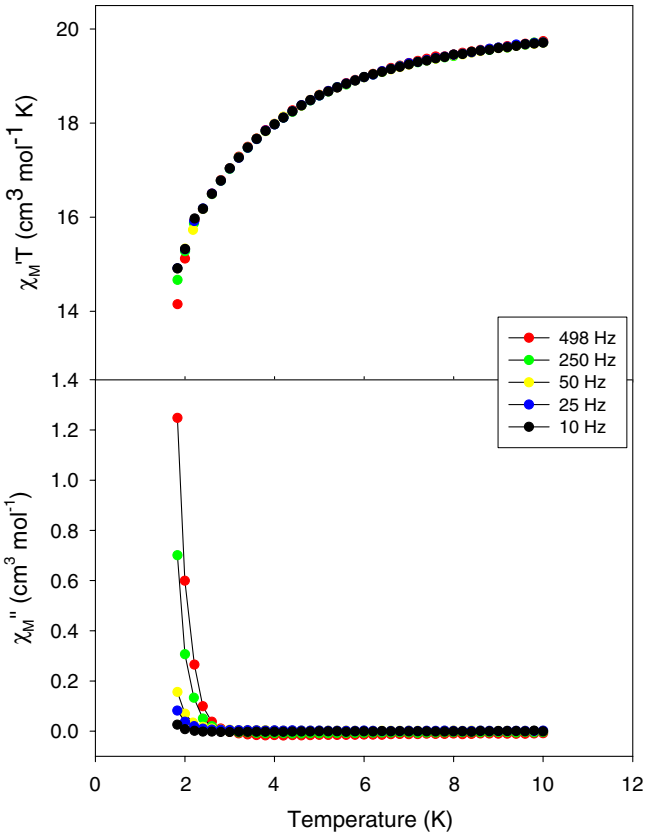

Fig. 5. Plots of the in-phase (χ'_M) as $\chi'_M T$ (top), and out-of-phase (χ''_M) (bottom) AC magnetic susceptibilities vs. T in a 3.5 G field oscillating at the indicated frequencies for complex **4**. The solid lines are visual aids.

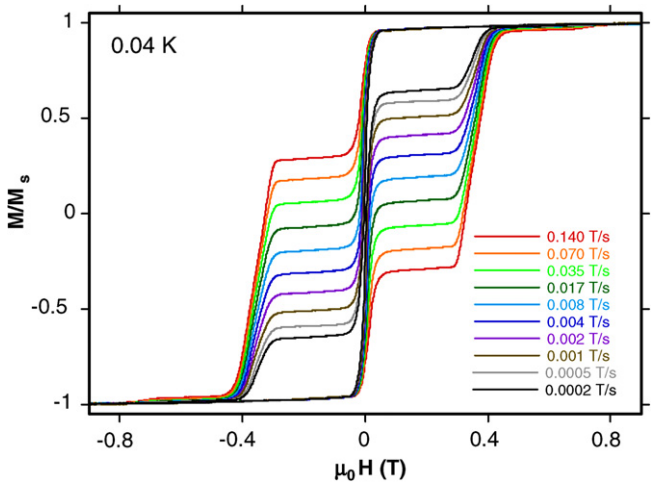

Fig. 6. Magnetization (M) vs. DC field hysteresis loops for a single crystal of $\mathbf{3} \cdot 3CH_2Cl_2$ at 0.04 K at the indicated field scan rates. The magnetization is normalized to its saturation value, M_s.

coordination of mpko$^-$ or ppko$^-$. In contrast, the oxide ion in **1**, **2** and related species is coplanar with the three metal ions. This distortion from planarity in **3**–**5** weakens the antiferromagnetic contributions (via $Mn^{III}_{d\pi}$–$O^{2-}_{p\pi}$–$Mn^{III}_{d\pi}$ orbital overlap) to the observed exchange between two Mn^{III} ions, and the latter (which is the sum of ferro- and antiferromagnetic contributions) becomes ferromagnetic leading to $S = 6$ ground states.

In summary, reactivity studies of the well known and well studied antiferromagnetically coupled $[Mn_3O(O_2CR)_6(py)_3](ClO_4)$ "starting materials" with 2-pyridyl oximes have led to a new family of triangular, oxide-centered, mixed carboxylate/2-pyridyloximate Mn(III) complexes that are ferromagnetically coupled with an $S = 6$ ground state. Complexes **3**–**5** are SMMs, the first for 3d metal complexes with a triangular topology. Given this success, the use of 2-pyridyl oxime ligands in Mn carboxylate chemistry continues to be investigated.

Acknowledgements

Th.C.S. and S.P.P. thank ESF, EPEAEK II, and particularly the Program PYTHAGORAS (Grant b.365.037), for funding the above work. G.C. thanks the NSF for support.

Appendix A. Supplementary material

CCDC 291916, 622143 and 623023 contain the supplementary crystallographic data in CIF format for $\mathbf{3} \cdot 3CH_2Cl_2$, $\mathbf{4} \cdot 1.2CH_2Cl_2 \cdot 1.4H_2O$ and $\mathbf{5} \cdot 2CH_2Cl_2$. These data can be obtained free of charge via http://www.ccdc.cam.ac.uk/conts/retrieving.html, or from the Cambridge Crystallographic Data Centre, 12 Union Road, Cambridge CB2 1EZ, UK; fax: (+44) 1223-336-033; or e-mail: deposit@ccdc.cam.ac.uk. Supplementary data associated with this article can be found, in the online version, at doi:10.1016/j.poly.2006.10.025.

References

[1] (a) For reviews, see: G. Christou, D. Gatteschi, D.N. Hendrickson, R. Sessoli, MRS Bull. 25 (2000) 66;
(b) G. Aromi, E.K. Brechin, Struct. Bond. 122 (2006) 1;
(c) R. Bircher, G. Chaboussant, C. Dobe, H.U. Güdel, S.T. Oshsenbein, A. Sieber, O. Waldmann, Adv. Funct. Mater. 16 (2006) 209;
(d) D. Gatteschi, R. Sessoli, Angew. Chem., Int. Ed. 42 (2003) 268.
[2] J.R. Friedman, M.P. Sarachik, J. Tejada, R. Ziolo, Phys. Rev. Lett. 76 (1996) 3830.
[3] W. Wernsdorfer, R. Sessoli, Science 284 (1999) 133.
[4] J.B. Vincent, H.-R. Chang, K. Folting, J.C. Huffman, G. Christou, D.N. Hendrickson, J. Am. Chem. Soc. 109 (1987) 5703.
[5] For a review, see: C.J. Milios, Th.C. Stamatatos, S.P. Perlepes, Polyhedron 25 (2006) 134, polyhedron report.
[6] Th.C. Stamatatos, D. Foguet-Albiol, C.C. Stoumpos, C.P. Raptopoulou, A. Terzis, W. Wernsdorfer, S.P. Perlepes, G. Christou, J. Am. Chem. Soc. 127 (2005) 15380.
[7] W. Liu, H.H. Thorp, Inorg. Chem. 32 (1993) 4102.
[8] R.D. Cannon, U.A. Jayasooriya, R. Wu, S.K. arapKoske, J.A. Stride, O.F. Nielsen, R.P. White, G.J. Kearley, D. Summerfields, J. Am. Chem. Soc. 116 (1994) 11869.
[9] W. Wernsdorfer, Adv. Chem. Phys. 118 (2001) 99.